Microstructure Scaling Properties and Fatigue Resistance of Pre-Strained Aluminium Alloys (Part 1: Al-Cu alloy)

C. Froustey, O. Naimark, M. Bannikov, V. Oborin

Title: Microstructure Scaling Properties and Fatigue Resistance of Pre-Strained Aluminium Alloys (Part 1: Al-Cu alloy)

Authors: C. Froustey, O. Naimark, M. Bannikov, V. Oborin

PII: S0997-7538(10)00096-3

DOI: 10.1016/j.euromechsol.2010.07.005

Reference: EJMSOL 2631

To appear in: *European Journal of Mechanics / A Solids*

Received Date: 6 March 2009

Revised Date: 13 July 2010

Accepted Date: 15 July 2010

Please cite this article as: Froustey, C., Naimark, O., Bannikov, M., Oborin, V. Microstructure Scaling Properties and Fatigue Resistance of Pre-Strained Aluminium Alloys (Part 1: Al-Cu alloy), European Journal of Mechanics / A Solids (2010), doi: 10.1016/j.euromechsol.2010.07.005

Microstructure Scaling Properties and Fatigue Resistance of Pre-Strained Aluminium Alloys (Part 1: Al-Cu alloy)

C. Froustey[a]*, O. Naimark[b], M. Bannikov[b], V. Oborin[b]

[a] Université Bordeaux 1, Arts et Metiers ParisTech, LAMEFIP, Esplanade des Arts et Métiers, 33405 Talence, France

[b] Institute of Continuous Media Mechanics of the Russian Academy of Sciences, 1 Acad. Korolev str., 614013 Perm, Russia

Abstract

The objective of this work is to provide the link between the fatigue behaviour of pre-strained aluminium alloys and the scaling properties of damage induced on the fracture surface. Fatigue tests performed on pre-strained aluminium alloys revealed a large difference in their residual fatigue resistance linked to the material: the Al-Cu alloy demonstrated a sharp decrease of HCF life-time due to the pre-straining whereas the insensitivity of the Al-Mg alloy was clear. For the Al-Cu alloy, the investigations made at a 'mechanical' scale allow us to associate the strain energy absorbed during the prior loading with the aspect of the surface and the residual HCF life-time. The statistical characterisation of the fatigue damaged zone was done from the measurement of the surface roughness. Scaling properties were established that allowed the conclusion of the universality of HCF damage kinetics as the mechanism controlling the sensitivity of Al-Cu alloy whatever the pre-straining history.

Keywords: Fatigue; Impact; Consecutive loadings; Damage tolerance; Scaling exponent; Aluminium alloy

1 Introduction

The interaction between the pre-loaded states and high cyclic fatigue (HCF) is of great interest. Low cycle fatigue (LCF) and quasi-static and dynamic pre-loadings can represent foreign object damage

*Corresponding author: Tel: + 33 5 56 84 53 67, Fax: + 33 5 56 84 53 66, E-mail address: catherine.froustey@lamef.bordeaux.ensam.fr

(FOD) for the application in the aircraft engine industry, for instance (Peters and Ritchie, 2000; Martinez et al., 2002). The natural tendency in the prediction of HCF failure for the pre-loaded materials is the development of the so-called 'damage tolerant' approach (DTA) based on the prediction of crack propagation to detectable flaw size (Nicholas, 1999; Ritchie and Lankford, 1986). In the comparison with LCF, HCF kinetics includes a relatively large fraction of life for the creation of damage to a detectable size. This results in a very small fraction of life-time remaining. Consequently, the estimation of the HCF life-time in the presence of damage from other sources is related to the capability of materials to resist in the conditions of initial or in-service damage. The concept of DTA needs a fundamental understanding of nonlinear aspects of damage-failure transition. It means that one of the main goals of DTA can be formulated as the way to improve the method of estimation of the HCF life-time, when the material capability is reduced by in-service loadings.

Much research has been conducted to identify and detect HCF damage in the early stages of total fatigue life and several types of fatigue damage related to different scales can be identified (Suresh, 1991): persistent slip bands (PSB), striations, micro-cracks formed at the interfaces between PSB and the matrix, damage at grain boundaries. Most of the damage is related to the defect range from 0.1 μm - 1 mm which is below the non-destructive evaluation limit ($\sim$ 1 mm). Moreover, it is generally observed that a component in service spends about 80% of its life-time in the formation of dislocation substructures and short crack growth. As a consequence, studies of multi-scale damage kinetics becomes an important part in the estimation of HCF life-time (Peters and Ritchie, 2000; Nicholas, 1999).

This research is devoted to the study of two aluminium alloys (Al-Cu and Al-Mg) that revealed qualitatively different fatigue responses on pre-strained states, depending on their compositions and hardening modes (Froustey and Lataillade, 2008). This paper concerns the Al-Cu alloy.

The first part presents the mechanical aspect: the experiments and the residual properties of the material after different configurations of pre-straining. The second part concerns the investigations made on the fracture surfaces to study scaling properties: the measurements on the roughness zones induced from the different types of damage. In the last part, a link between the mechanical behaviour, the damage induced from the pre-loadings and the microstructure properties (scaling invariance) is proposed.

Impact tensile – fatigue and quasi-static tensile – fatigue loadings have been carried out on Al-Cu alloy. These loadings were chosen to represent the current sequences found during the life of a structural component in the transportation sector.

2.1 Material and experimental set-up

2.1.1 Material and specimen

The 2017A-T3 is an aluminium-copper alloy, largely present in aircraft structures. It is a structural hardening material. The T3 denotes a quenched, cold work hardening and naturally aged state. The microstructure consists of two phases: α (or Al-Cu phase), which is the copper solution in the aluminium matrix and β (Al_2Cu phase), the second phase of precipitates. The β phase is finely dispersed and has a size in the range of about $10{\cdot}10^{-9}$ m. In addition, dispersoids and inter-metallic inclusions are contained in the material. The mean size of these precipitates varies from about 100 to $500{\cdot}10^{-9}$ m for the first type to about 4 to $5{\cdot}10^{-6}$ m for the second type.

The chemical composition (in weight %) of the alloy is provided in Table 1 and its tensile properties are summarized in Table 2.

The geometry of the specimens, which must be adaptable for both fatigue and impact testing machine is given in Fig. 1. They were drawn with a toroidal cross-section to localize the fatigue damage and to minimize the fatigue scatter.

2.1.2 Testing machines

Impact device:

The impact loadings were carried out using an inertial flywheel. The principle and associated measurement techniques of this device are described in (Froustey et al., 2007). It is possible to stretch specimens at medium or high strain rates (up to 10^3 s^{-1}). Its essential elements are a wheel and a pendular system (Fig. 2).

The wheel has a large size (1 metre diameter), a large mass (620 kg) and is equipped with a hammer on its circumference. The pendular system consists of a 3 meter long bar: one end is used as the pivot and the specimen and an anvil are attached to the other end. To store energy, the wheel turns freely

until reaching the selected speed, then the pendular system is lowered. The hammer impacts the anvil and the specimen is strained.

Prior tensile loadings (impact and quasi-static):

To carry out prior impact loadings, a specific device coupling a displacement limit stop and a mechanical fuse have been designed (Fig. 3). After the hammer impingement on the anvil, the specimen is stretched until the washers hit against the frame. The fuse, which makes the junction between the two parts of the extension component which is therefore the weakest element, and it therefore breaks. Before the test, the space between the washers and the frame was regulated with calibrated spacers: a controlled extension (DL) was imposed on the gauge zone of the specimen. Various values of prior elongation were applied (DL = 0.5, 1 and 1.5 mm), characterized by the k factor, which was determined as the imposed elongation over the total impact failure elongation (in percent). k values were respectively 25, 50 and 75%. The tests were performed at about 5 ms^{-1} that gave a strain rate of about 300 s^{-1} in the central zone of the specimens.

Prior quasi-static loadings were carried out on a classic tensile machine (Instron 8500 series), using the same specific device. To characterize the strain rate effect of pre-damage, the same elongation values were used.

Characteristic dynamic and quasi-static diagrams for Al-Cu alloy are presented in Fig. 4 and the markers (DL) show the pre-loading configurations.

Fatigue device:

The fatigue tests were done on a resonant electromagnetic machine (Amsler Vibrophore) with a controlled force, for fully reversed tensile-compression loading. The principle is to set and maintain a spring-mass system, in which the specimen represents the spring, in a resonant state. The frequency of oscillations is recorded, which makes it possible to detect damage occurrence in the specimen: the appearance of fatigue cracks will cause a decrease of its stiffness and consequently of the oscillation frequency. The frequency shift was used as a test-stop and fixed at 0.4 Hz, equivalent to a crack section of about 2 to 4 mm^2.

The stress level chosen for the study of the residual fatigue behaviour corresponds to a life time of about $2{\cdot}10^5$ cycles (220 MPa) for the damage free material. In this field, the number of cycles to failure (N_F) follows a log-normal law, then the stress level was imposed and N_F was recorded. Because of the fatigue scatter, five to ten samples were tested under each configuration that allows us to determine the mean value and the associated standard deviation of N_F.

2.2 Residual high cycle fatigue properties

2.2.1 Residual fatigue life

The results are summarized in Fig. 5. It represents the mean value (markers) and the associated standard deviation (vertical lines) of the number of cycles to failure, versus the defined k factor. (To compare the difference in behaviour, the results obtained on the Al-Mg aluminium alloy have been plotted on the same figure: its insensitivity to the pre-tensile loading is obvious). Looking at the Al-Cu results, it can be noticed: 1) N_F is highly influenced by the pre-tensile loadings. 2) No influence of the pre-loading strain rate on N_F can be observed: pre-straining from quasi-static loading or pre-straining from dynamic loading result in roughly the same number of cycles to failure. Statistical test methods (such as the Snedecor method (Snedecor and Ochran, 1989)) makes it possible to compare with confidence the mean values of the normal distributions (the value between brackets represents the confidence threshold that it means the percent of probable error): 1) each pre-tensile configuration and whatever the strain rate loading leads to a residual fatigue life different from the undamaged material (1%). 2) for a given strain rate, the residual fatigue life from the various configurations (k value) shows a difference (1%). 3) for a given pre-tensile (k value), the residual fatigue life is not different versus the strain rate (1%).

The determination of the strain energy absorbed during the prior loading and the failure surfaces observation make possible a part-understanding of these results.

2.2.2 Strain energy absorbed

For the damage free material, the strain rate effect between quasi-static and impact loadings appeared to have a weak effect on the macroscopic properties (Fig. 4). It has been evaluated with an increase of 15% for the yield stress (420 to 480 MPa) and 10% for the maximum tensile strength. The test results under consecutive loadings show that the same pre-stretching leads to the same residual behaviour. This behaviour is independent of the pre-loading strain rate. Only the value of the lengthening reached can have an influence. As the mechanical behaviour is similar, the strain energy absorbed during the first loading reaches about the same value for a given elongation (Table 3).

As a consequence, it seems that the fundamental parameter which determines the residual behaviour is the value of the absorbed energy. If the difference in strain rate, which modifies the pair

(number of defects, size of defect), leads to the same energy, the residual material behaviour is the same. The material loses the memory of the process which led to absorbing it.

2.2.3 Failure surface observations

Fig. 6 shows the pictures of the fatigue fracture surfaces of the specimens made in a scanning electron microscope (SEM). Whatever the sequential loading, fracture surfaces show 45° tilted planes (Fig. 6a): the first plane (mark 1 and mark 2) reveals the fatigue signature, the second (mark 3) results from the section of the specimen (to make possible the observations after the consecutive loadings).

Two zones can be noticed on the fatigue fracture region (mark 1 and mark 2). For Fig. 6b (magnification of mark 1), taken near the external surface, the profile reveals mainly randomly distributed strain lines and micro-cracks, it corresponds to the initiation fatigue zone and no difference appears whatever the sequential loading.

The second region (mark 2) is largely different in relation to the pre-tensile elongation (k values), but is the same whatever the strain rate of the prior elongation (QS or 300 s^{-1}). Fig. 6c-f show the observed profiles for k=0%, k=25%, k=50% and k=75% respectively. Each fracture surface consists of intergranular fracture with striations and ductile fractures with a rough surface. For k=0%, Fig. 6c shows a large region of striations with various propagation directions and partly of small dimples; these dimples contained the intermetallic inclusions (spheres on the image). k=25% (Fig. 6d) is characterized by a large population of voids with the same size and shape ($\approx 6\,\mu$m) and the plane regions reveal an intergranular fracture. Fig. 6e for k=50%, shows a profile with voids of small size and voids of large size; plane zones are numerous with random orientations. For k=75% (Fig. 6f), dimples or voids of small size have completely disappeared. Pockets of large voids ($\approx 40\,\mu$m) and dimples ($\approx 10\,\mu$m) are found randomly distributed among series of regular striations. Many micro-cracks start from these voids and dimples.

The SEM observations made on zone 2 of the fracture surfaces of the specimens are completely in agreement with the mechanical test results: for a given k value, the profiles are the same whatever the strain rate and a given type of profile can be linked with a given residual life-time.

Finally, these investigations allow us to associate the strain energy with the aspect of the surface and the residual HCF life-time. The aim is now to establish a link between the pre-damaged state and the final state of the material.

3 Criticality of damage-failure transition and scaling characteristics for HCF life-predictions

3.1 Scaling characteristics of fracture surface

Quantitative fractography has been recently a useful tool for understanding the link between defect induced heterogeneities, evolution of dislocation ensembles, micro-cracking and fracture mechanisms. The fracture surface and the free surface (that can be sensitive to structure rearrangement during deformation) morphologies of strained materials have been studied with different experimental techniques (Bouchaud, 1997; Carpinteri et al., 1999; Zaiser, 2006). High resolution techniques (atomic force microscopy (AFM), scanning white-light interferometry (SWLI)) can be used as a quantitative analysis method. A correlation between the measured roughness (induced by damage) and the macroscopic mechanical properties can be established.

The basis for this analysis is the feature of surfaces to show scaling properties, it means that they exhibit self-affine scaling invariance over a wide range of length scales. This was shown first by Mandelbrot et al. (Mandelbrot et al., 1984) by the study of correlation (fractal) properties of fracture surface roughness.

The fracture surface reveals statistical self-similarity through an affine transformation: $(X, Y, Z) \rightarrow (bX, bY, b^{\zeta}Z)$, where Z is the height, $r = \sqrt{X^2 + Y^2}$ is the horizontal point along the surface profile direction; ζ is the so-called roughness exponent or Hurst exponent.

The range of ζ lies between the values 0 and 1 and has the following link with the fractal dimension of the surface morphology: $d_F = 3 - \zeta$. The self-affine (fractal) scaling expands up to a distance of characteristic length, called the correlation length, beyond which: $\zeta = 1$, that corresponds to a regular surface with dimension $d_F = 2$.

There are different methods of estimating the roughness exponent (Schmittbuhl et al., 1995). One of the simplest quantifiers determines how the height Z at R is correlated at R+r. The affine transformation implies that the mean height differences h(r) versus the separation distance r is given by

$$h(r) = \left\langle \left(Z(R+r) - Z(R) \right)^2 \right\rangle_R^{1/2} \approx r^{\zeta} ,$$

ζ can be obtained by plotting h(r) versus r.

The double logarithmic plots of experimentally measured h(r) versus r exhibit an area of constant slope. This linear regime appears along the scales between 0.05 and 50 μm related to the ranges

of resolution of the analysis method (AFM+SWLI). This scaling regime can be associated with the property of self-similarity of multi-scale damage kinetics that consists of the evolution of different dislocation substructures and micro-cracks.

For example, a correlation was established between the roughness exponent ζ and the fracture toughness K_{1c} . The decrease of ζ from 0.8 to 0.6 was observed, corresponding on the transition from dynamic crack propagation to the regime of crack kinetics that is a characteristic for HCF (Morel et al., 2000; Naimark et al., 2000; Naimark and Uvarov, 2004).

For the surfaces with deformation (strain localization) traces, the roughness exponent remains spatial invariant too. As a consequence, a relation between the surface profile and the distortion related to the plastic strain localization can be determined also in terms of roughness exponent. The link between the height Z of the surface profile and the strain fluctuations can be expressed as $\frac{\partial Z}{\partial r} \sim \varepsilon(r) - <\varepsilon> \approx \varepsilon(r)$.

The probability distribution function of the surface height differences demonstrates also the self-affine scaling. The distribution $P_R(\Delta Z)$ is collapsed by the re-scaling $P_R(\Delta Z) = P_{R'}((\frac{r}{r'})^{\zeta}\Delta Z)$ with a typical roughness exponent $\zeta \approx 0.75$.

This fact and the universality of the scaling exponent along large scales allowed the conclusion that crack propagation kinetics can be considered in the framework of a large group of critical phenomena – the structural-scaling transitions (Williford, 1998; Carpinteri, 1994; Naimark, 2004; Paggi and Carpinteri, 2009), that describe the scenario of damage evolution.

An accurate estimation of the scaling exponent was proposed in (Carpinteri et al., 1999; Zavarise et al., 2007). It can give physical implication of universality classes related to the failure scenario and the role of the pre-loaded microstructure on the 'yielding transition' of the deforming materials to fracture (Naimark, 2004; Naimark et al., 1998). It can be applied to identify the critical conditions of the fatigue crack advance and life-time prediction.

3.2 Scaling analysis of HCF fracture surface after the consecutive loadings

FOD implies a combination of a residual stress state induced by micro-cracks and micro-structural damage induced by plastic flow. This state can be imitated by the pre-straining of specimens. The scaling analysis of damage induced roughness was used to establish the variance of the pre-loaded states on the following fatigue resistance.

3.2.1 Hurst exponent determination

Fig. 7 shows a 3D image of the fracture surface scanned by a high resolution interferometer-profiler (SWLI, New View 5010). The characteristic zone 2 (Fig. 8 and Fig. 6c-f) that reflects the fatigue damage scenario for different pre-strained material microstructure was investigated.

Scanning areas with a size from 100x100 to 600x600 μm^2 were distributed in this zone. One-dimensional traces of scanning in an area has the orientation along the radial direction starting from the boundary of zone 1 (the fatigue crack origination) in the mean direction of crack propagation. From 20 to 25 one-dimensional traces for each area were recorded and 5 to 6 areas were scanned per specimen. Fig. 8 gives a schematic illustration of the scanning procedure and Fig. 9 shows a characteristic plot of one-dimensional roughness in an area (350x350 μm^2) in the zone 2. The vertical resolution of the heights Z was in the range of 1 nm and the horizontal resolution along the traces from 1 to 5 μm (depending on the area size).

In order to determine the roughness exponent ς of the profiles recorded, the Hurst method was used, where the following quantity was computed (Bouchaud, 1997; Zaiser, 2006; Naimark et al., 1998):

$$Z_{max}(r) = \left\langle max\left((Z(r^{'})\right)_{R<r^{'}<R+r} - min\left((Z(r^{'})\right)_{R<r^{'}<R+r} \right\rangle_{R}; \tag{1}$$

$$Z_{max}(r) \propto r^{\varsigma} \tag{2}$$

$Z_{max}(r)$ is the difference between the maximum and minimum heights Z within the bands averaged over all possible origins R of the bands, belonging to the profiles.

Fig. 10 shows an exemple (QS + Fatigue sequence) of the double logarithmic plots of roughness data in terms of equations 1 and 2. The linear slope of $\ln Z_{max}(r)$ vs $\ln(r)$ allowed the estimation of the roughness exponent as the scaling invariant in the range of r; the resolution of the set-up make it possible to assume the existence of the upper and lower bounds for the definition of the power-law scaling between Z and r. Table 3 and Fig. 11 give the mean values of the Hurst exponent for each type of sequence loading. The values of ζ reflect the regime of crack kinetics that is characteristic for HCF (about 0.6 - 0.7).

3.2.2 Schematic damage evolution

From Table 3 and Fig. 11, it can be observed that there is a slight variation of the Hurst exponent for the specimens with different pre-loading histories. The invariance of the ζ values reflects the unified

scenario of damage accumulation and transition to failure. As a consequence, all the pre-loading states (k values) and the ζ position can be plotted on the same curve of damage evolution. Fig. 12 shows a scheme of this scenario where N_{F0} represents the number of cycles to failure for the damage free material, N_{Fk} the residual number of cycle after a prior elongation and ζ measurement gives the image of the end of process.

The role of the states of the pre-loaded microstructure can be analysed in terms of the initial conditions for the damage parameter. Such analysis explains the fatigue life-time sensitivity to the consecutive loading. This conclusion has important consequences for the formulation of constitutive equations linking the stress-strain material response and damage kinetics.

The stress-strain diagram of the Al-Cu reveals a weak strain rate sensitivity (Fig. 4). The residual fatigue behaviour of the pre-strained material shows also insensitivity to the strain rate (Fig. 5). However, the damage state (number of defects, size of defects) is always sensitive to the strain rate. This feature of damage-failure transition can be presented in an appropriate form of damage evolution equation. Such equations can reflect, in a large range of strain rates, the specific non-linearity of the free energy release with the unified scenario of multi-scale damage-failure transition (Naimark, 2004; Naimark et al., 1998). The establishment of this type of universality can be crucial to implement the conception of the damage tolerant approach for the estimation of fatigue life in the presence of FOD.

In contradiction with this alloy, Al-Mg alloy demonstrates qualitative different scaling behaviour (the variety of scaling exponent for different pre-strained states). It shows also an important modification on its stress-strain diagram due to the strain rate. As a consequence, it is possible to observe extremely low sensitivity to the pre-loading history (Fig. 5). This feature can be linked with a selected 'criticality' scenario of structure evolution that is characteristic for these types of alloys revealing different types of scaling properties for characteristic ranges of strain rates.

4 Discussion and conclusions

The microstructural properties of the fracture surfaces for Al-Cu alloy revealed the scaling universality in term of the Hurst exponent. The Hurst exponent invariance reflects the self-similar scenario of damage kinetics related to long-range correlation properties of defects providing damage-failure transition under HCF crack propagation. High sensitivity of HCF life-time to the pre-strained states for the Al-Cu alloy can be linked with the unit multi-scale channel of the free energy release that provides self-similarity of micro-structural changes over a long range of spatial scales. This scaling universality can be reflected in the appropriate form of damage accumulation law that links the non-linearity of energy

release and structural relaxation due to the generation of dislocation substructures and micro-cracks. This approach will be presented after consideration of Al-Mg alloys revealing a qualitative distinct response to HCF after pre-straining (Froustey and Lataillade, 2008).

The formulation of structure sensitive phenomenology of the damage-failure transition will reflect the mentioned self-similarity and can be considered as the effective way to realize the damage tolerance conception for HCF.

Based on the study of the role of the pre-straining of two aluminium alloys (Al-Cu and Al-Mg) for high cycle fatigue, involving the scaling analysis of damaged induced roughness in the fatigue zone of the fracture surface, the following conclusions can be made:

- Two mentioned alloys have qualitative different fatigue responses to quasi-static and dynamic pre-loadings. That reflects distinct sensitivity to HCF resistance relative to possible FOD.
- The study of damage induced microstructure in the HCF damage zone on the fracture surface of Al-Cu alloy, revealed a slight variation of spatial invariant (the Hurst exponent) for different pre-loading conditions. That reflects the universality of damage kinetics related to the unit scenario of multi-scale free energy release.
- The sensitivity of HCF of Al-Cu alloy to the pre-strained states can be reflected in an appropriate form of damage evolution equation, when the following HCF damage scenario can be estimated by simulation of pre-strained damage states.

References

Bouchaud, E., 1997. Scaling properties of cracks. J. Phys. Condens. Matter 9, 4319–4344.

Carpinteri, A., 1994. Scaling laws and renormalization groups for strength and toughness of disordered materials. Int. J. Solids Struct. 31, 291–302.

Carpinteri, A., Chiaia, B., Invernizzi, S., 1999. Three-dimensional fractal analysis of concrete fracture at the meso-level. Theor. Appl. Fract. Mech. 31, 163–172.

Froustey, C., Lambert, M., Charles, J. L., Lataillade, J. L., 2007. Design of an impact loading machine based on a flywheel device: application to the fatigue resistance of the high rate pre-straining sensitivity of aluminium alloys. Exp. Mech. 47 (6), 709–721.

Froustey, C., Lataillade, J. L., 2008. Influence of large pre-straining of aluminium alloys on their residual fatigue resistance. Int. J. Fatigue 30, 908–916.

Mandelbrot, B. B., Passoja, D. E., Paullay, A. J., 1984. Fractal character of fracture surfaces of metals. Nature 308, 721–722.

Martinez, C. M., Eylon, D., Nicholas, T., Thompson, S. R., Ruschau, J. J., Birkbeck, J., Porter, W. J., 2002. Effects of ballistic impact damage on fatigue crack initiation in Ti-6Al-4V simulated engine blades. Mater. Sci. Eng. A325, 465–477.

Morel, S., Schmittbuhl, J., Bouchaud, E., Valentin, G., 2000. Scaling of crack surfaces and implications for fracture mechanics. Phys. Rev. Lett. 85 (8), 1678–1681.

Naimark, O. B., 2004. Defect induced transitions as mechanisms of plasticity and failure in multifield continua. In: Capriz, G., Mariano, P. M. (Eds.), Advances in Multifield Theories of Continua with Substructure. Boston, Ch. 4, pp. 75–114.

Naimark, O. B., Davydova, M., Plekhov, O. A., 1998. Failure scaling as multiscale instability in defect ensemble. In: Frantziskonis, G. N. (Ed.), PROBAMAT-21 Century: Probabilities and Materials. NATO Science Series. Kluwer Academic Publishers, Netherlands, pp. 127–142.

Naimark, O. B., Davydova, M., Plekhov, O. A., Uvarov, S. V., 2000. Nonlinear and structural aspects of transitions from damage to fracture in composites and structures. Comput. Struct. 76 (1-3), 67–75.

Naimark, O. B., Uvarov, S. V., 2004. Nonlinear crack dynamics and scaling aspects of fracture (experimental and theoretical study). Int. J. Fract. 128 (1-4), 285–292.

Nicholas, T., 1999. Critical issues in high cycle fatigue. Int. J. Fatigue 21, 221–231.

Paggi, M., Carpinteri, A., 2009. Fractal and multifractal approaches for the analysis of crack-size dependent scaling laws in fatigue. Chaos Solitons Fractals 40, 1136–1145.

Peters, J. O., Ritchie, R. O., 2000. Influence of foreign object damage on crack initiation and early crack growth during high-cycle fatigue of Ti-6Al-4V. Eng. Fract. Mech. 67, 193–207.

Ritchie, R. O., Lankford, J., 1986. Small fatigue cracks: A statement of the problem and potential solutions. Mater. Sci. Eng. 84, 11–16.

Schmittbuhl, J., Vilotte, J. P., Roux, S., 1995. Reliability of self-affine measurements. Phys. Rev. E 51 (1), 131–147.

Snedecor, G. W., Ochran, W. G., 1989. Statistical methods. Ames: Iowa State University Press, 8th ed, ISBN: 0-8138-1561-4.

Suresh, S., 1991. Fatigue of Materials. Cambridge-University Press, Cambridge, ISBN: 0-521-36510-4.

Williford, R. E., 1998. Multifractal fracture. Scripta Metal. Mater. 22, 1749–1754.

Zaiser, M., 2006. Scale invariance in plastic flow of crystalline solids. Adv. Phys. 55 (1-2), 185–245.

Zavarise, G., Borri-Brunetto, M., Paggi, M., 2007. On the resolution dependence of micromechanical contact models. Wear 262, 42–54.

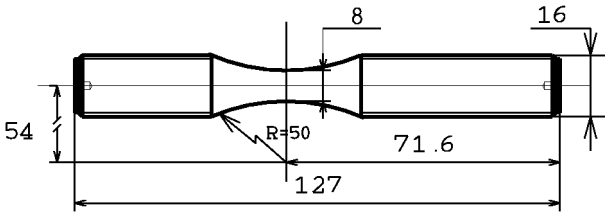

Figure 1: Specimen geometry (dimensions in mm).

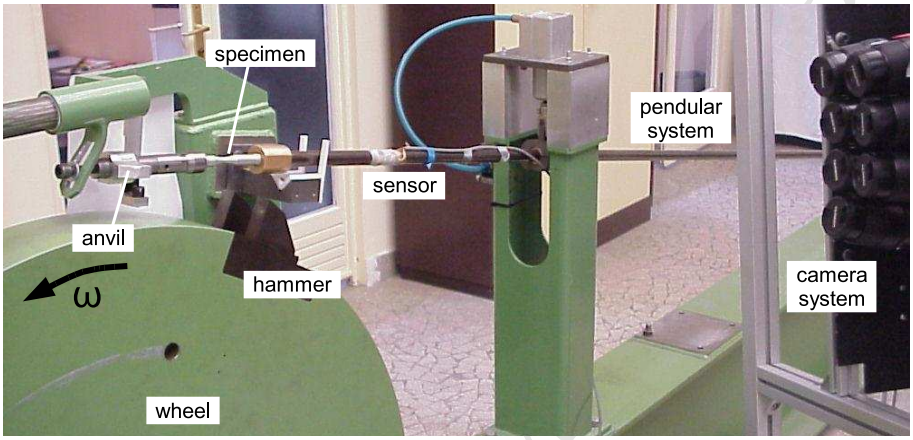

Figure 2: Impact device: the flywheel.

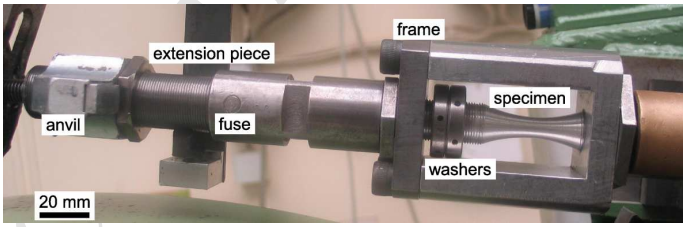

Figure 3: Interrupted testing device to carry out prior impact and prior quasi-static loadings.

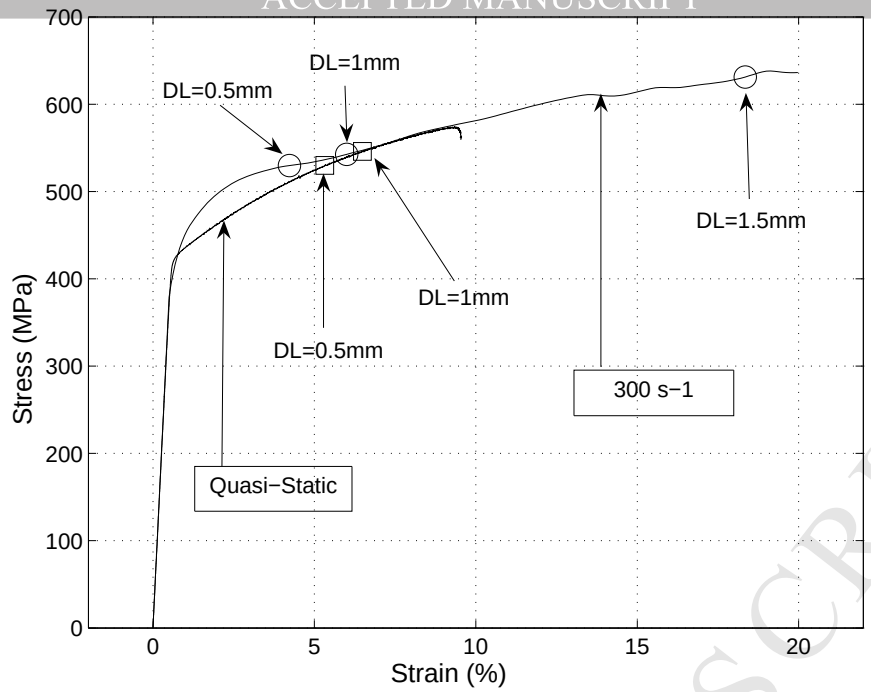

Figure 4: Quasi-static and dynamic diagrams for Al-Cu alloy. DL indicates the pre-straining monitored before loading.

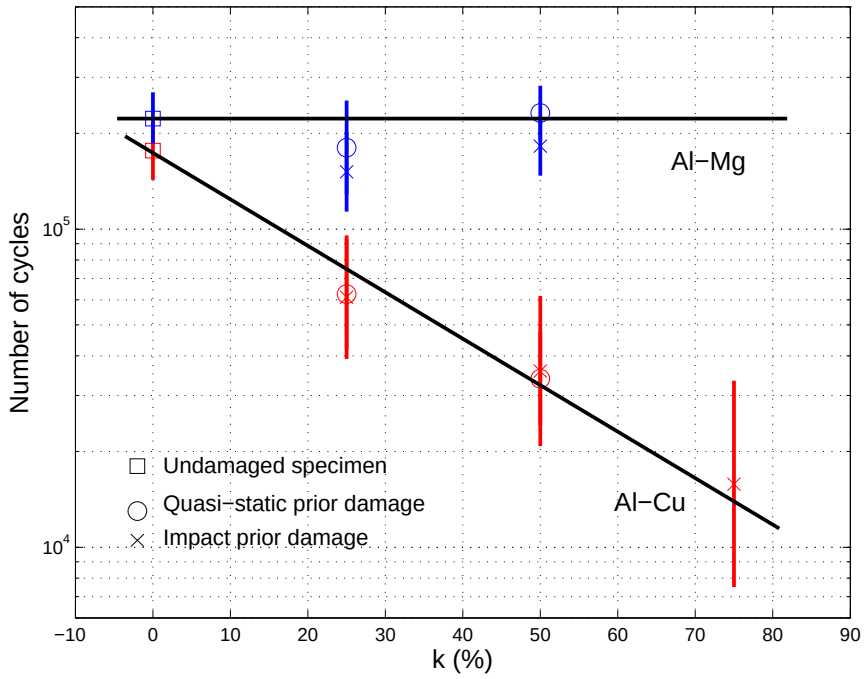

Figure 5: Residual fatigue behaviour after quasi-static and impact pre-loading.

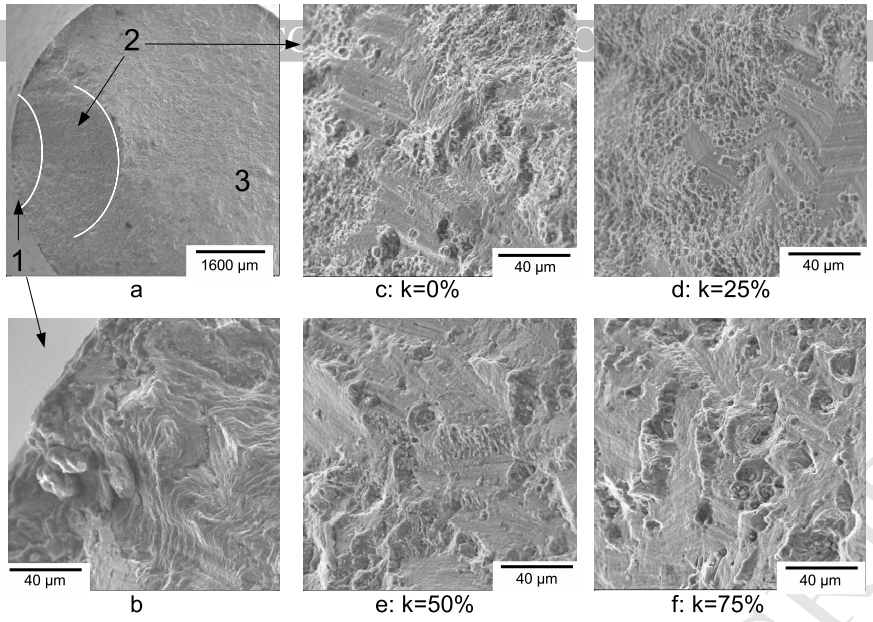

Figure 6: Al-Cu aluminium alloy: SEM observations of the failure surfaces after impact-fatigue or quasi-static-fatigue consecutive loadings.

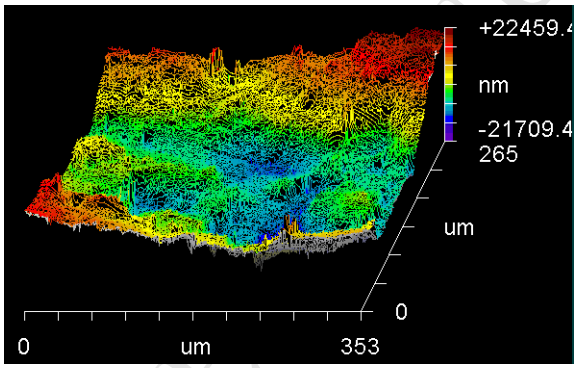

Figure 7: Characteristic 3D-image of fracture surface roughness (zone 2) after New View scanning

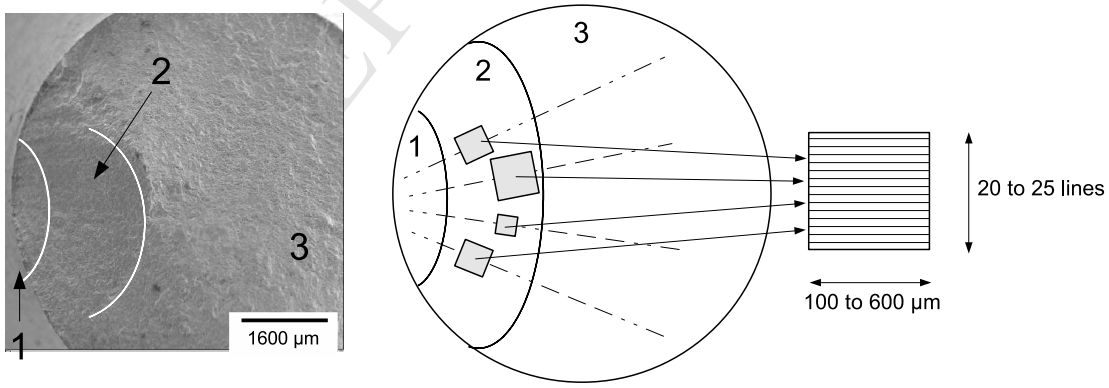

Figure 8: The characteristic zone of the fatigue damage scenario and a schematic illustration of New View scanning procedure.

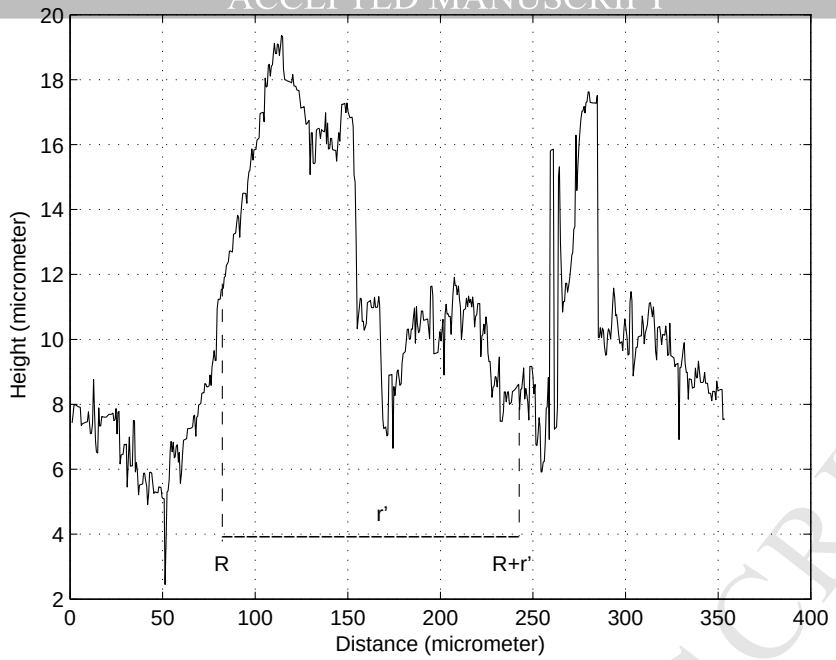

Figure 9: Characteristic plot of one-dimensional roughness in zone 2.

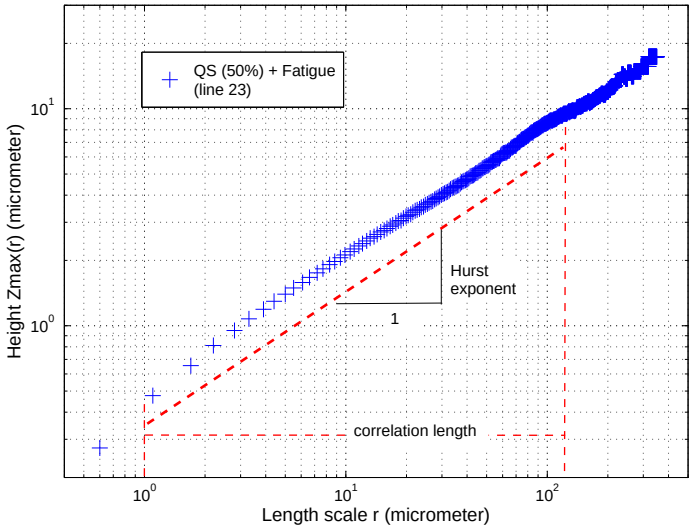

Figure 10: Scale invariance plot $ln\, Z_{\max}(r)$ vs $ln\, r$.

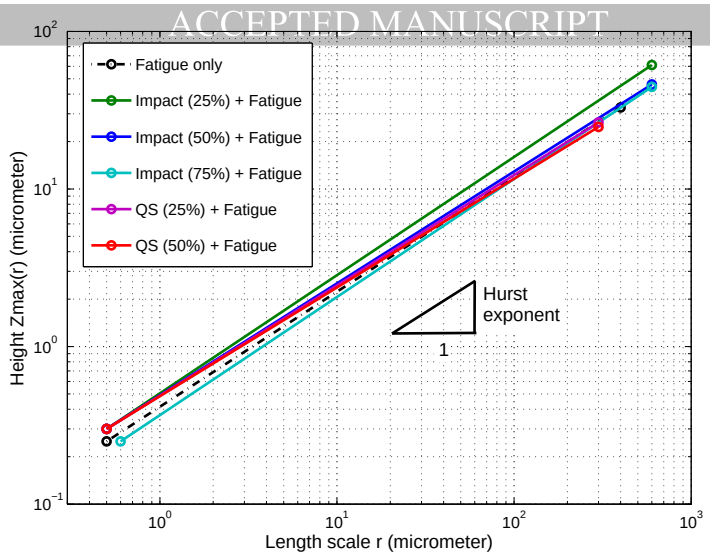

Figure 11: Mean values of the Hurst exponent for each type of sequence loading (scale invariance plot $ln\, Z_{\max}(r)\ vs\ ln\, r$)

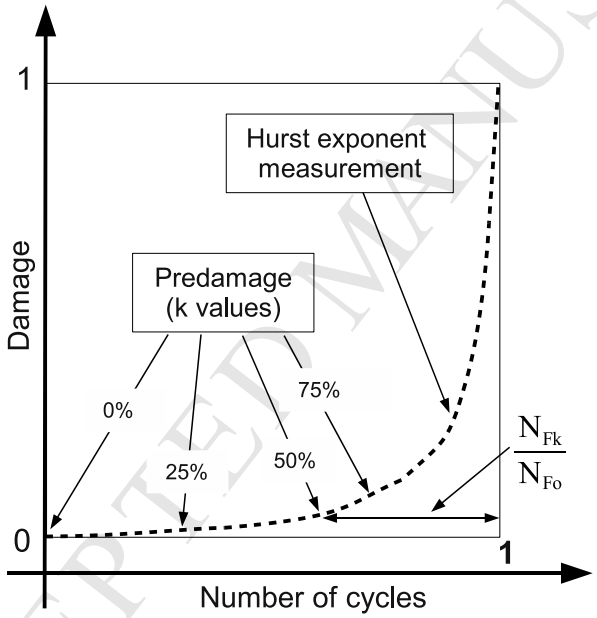

Figure 12: Schematic damage evolution in pre-strained Al-Cu aluminium alloy.

Alloy	Cu	Mg	Mn	Si	Fe	Zn	Cr	Ti + Zr
Al-Cu (2017A-T3)	3.5-4.5	0.4-1.0	0.4-1.0	0.2-0.8	$\leq$0.7	$\leq$0.25	$\leq$0.1	$\leq$0.25

Table 1: Chemical composition (in weight %)

Alloy	Elastic modulus (GPa)	Yield stress (MPa)	Tensile strength (MPa)	Elongation (%)
Al-Cu (2017A-T3)	75	427	573	13

Table 2: Quasi-static tensile characteristics

k% [DL (mm)]	Prior strain rate $\dot{\varepsilon}\,(s^{-1})$	Strain energy $W_p\,(10^6 J/m^3)$	Sequence loading	Hurst exponent
0% [0mm]	0	0	Fatigue only	0.67 $\pm$ 0.01
25% [0.5mm]	QS	24.1	QS + Fatigue	0.68 $\pm$ 0.01
25% [0.5mm]	300	19.5	300 s^{-1} + Fatigue	0.65 $\pm$ 0.01
50% [1mm]	QS	30.4	QS + Fatigue	0.66 $\pm$ 0.01
50% [1mm]	300	29	300 s^{-1} + Fatigue	0.64 $\pm$ 0.01
75% [1.5mm]	300	102.4	300 s^{-1} + Fatigue	0.71 $\pm$ 0.01

Table 3: Plastic strain energy absorbed during pre-stretching and values of the Hurst exponent given the sequence loadings